AREVA

ANP-10297 R0
Supp.1 R0 Q1NP
Revision 0

Response to Request for Additional Information – ANP-10297PA Supplement 1

The ARCADIA® Reactor Analysis System for PWRs Methodology Description and Benchmarking Results

May 2017

AREVA Inc.

Nature of Changes

Item	Section(s) or Page(s)	Description and Justification
1	All	Initial Issue

Contents

List of Tables

List of Figures

Nomenclature

Acronym	Definition
AFD	Axial flux difference
BOC	Beginning of cycle
CP	Collision probability
EOC	End of cycle
IDT	Integro-differential transport
MOC	Middle of cycle
NRC	U.S. Nuclear Regulatory Commission
RAI	Request for additional information
TR	Topical report

Introduction

The United States Nuclear Regulatory Commission (NRC) provided a request for additional information (RAI) regarding the topical report ANP-10297PA Revision 0 Supplement 1P, Revision 0 (Reference 1) in Reference 2. A total of ten questions were received from the NRC.

The following sections document the responses to the ten NRC questions.

1.0 RAI 1

Question:

Section 2.6.1 of the TR discusses the implementation of a model in APOLLO2-A for the generation of spacer grid form functions. These spacer grid form functions are used to produce spacer grid factors that mimic the behavior fuel assembly spacer grids have on assembly flux distributions and pin power in both steady state and transient core calculations. However, the actual nature of the spacer grid form functions and how they produce grid factors is not discussed in sufficient detail for the NRC staff to assess the range of applicability of the functions or the physical principles they utilize. Provide a mathematical description of the form functions, the grid factors, and the shape of the grid effect. If the form functions are comprised of a series of parameters (e.g., parameters describing flux suppression up/downstream of the grid), then also provide a mathematical description of how these parameters are generated.

Response:

Spacer grid form factors are generated with APOLLO2-A using [

] is depicted graphically in Figure 1-1.

The 1D geometry is composed of [

] The 1D flux is normalized to obtain the requested power:

[ ]

where

[ ]

[ ]

Different power terms are calculated using the final normalized flux and the following equations:

[

]

where

[

]

Changes in isotopics, which affect the self-shielding, will produce different cross sections as the lattice is depleted. [

]

[

]

[

]

where the two [ ] are:

[

]

[

] The spacer grid form functions are determined at various burnup levels and axial positions. [ ] locations are considered in developing the form functions:

[

]

[

[

] The cut-off energy between the thermal and fast energy groups is [

] An example of form functions generated using APOLLO2-A is shown below, [ ]:

[

]

The above form factors are also shown graphically in Figure 1-2, [

]

The APOLLO2-A generated spacer grid coefficients are converted to spacer grid depression factors using the following formula:

[ ]

where

[ ]

Spacer grid form functions can be calculated with APOLLO2-A for any fuel assembly type, spacer grid type, spacer height, boron concentration, and moderator temperature.

Figure 1-1
[ ] for Spacer Grid Form Factors Generation

Figure 1-2
Example of Spacer Grid Form Functions Generated with APOLLO2-A

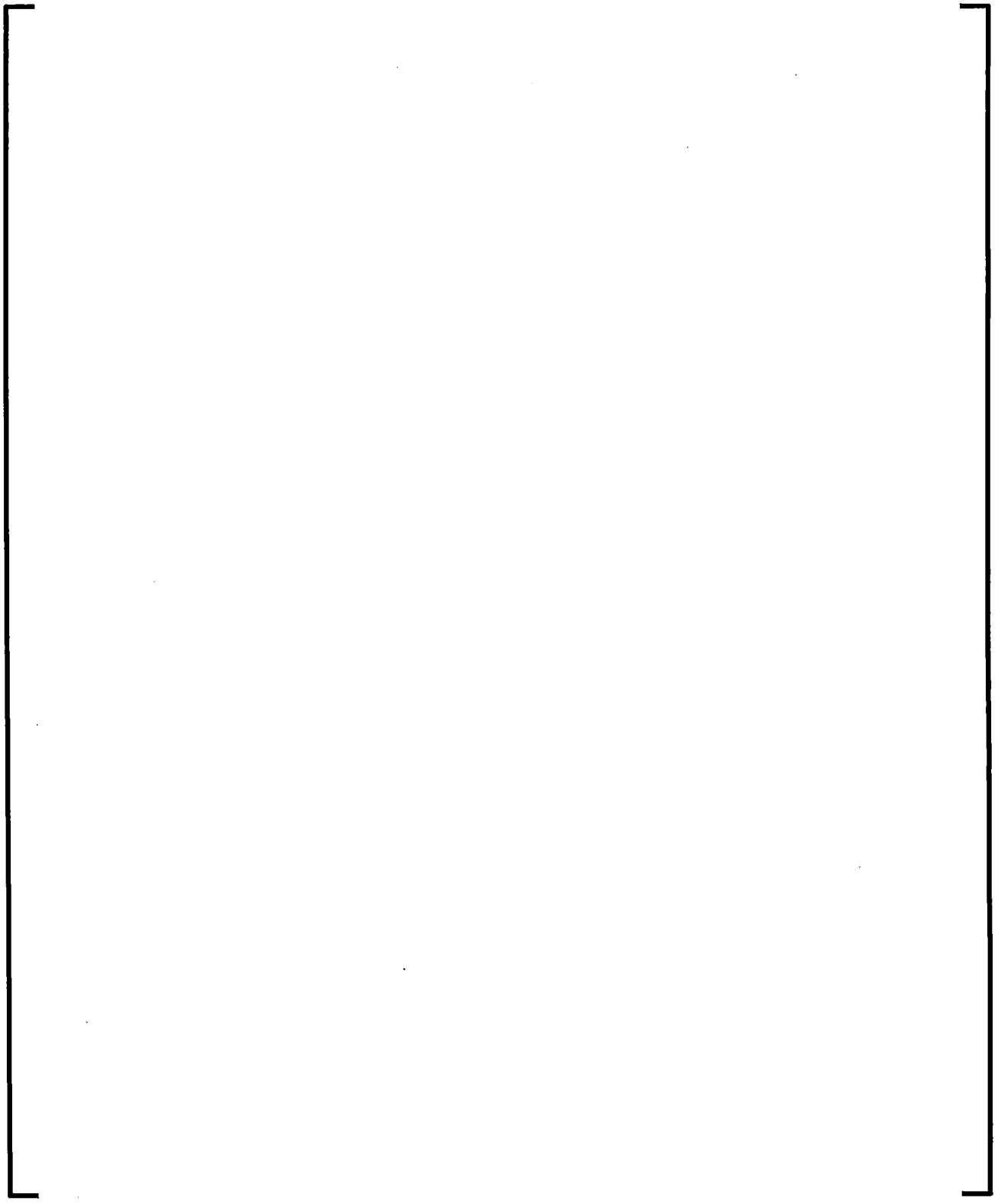

2.0 RAI 2

Question:

Section 2.6.1 indicates that [

] ?

Response:

[ ] were used in the topical report. The sensitivity of Fq with respect to different grid types was investigated during the development of the spacer grid model. A total of [ ] different grid models and grid factors were generated. These grid models were used in [ ] different fuel assemblies at different times during several cycles.

Table 2-1 provides a list of the evaluation cases. These cases include various fuel assembly types (enrichments, gadolinia content), actual spacer grids and a range of fuel assembly and cycle burnup values.

Table 2-1
Classification of Evaluated Cases

[

]

A total of [ ] sets of grid coefficients were generated using APOLLO2-A. Table 2-2 provides the characteristics of the grid coefficient sets. Several grid types were used along with variation in the [ ] used to generate the grid coefficients.

Table 2-2
Spacer Grid Coefficient Sets

[

]

The impact of the various Inconel spacer grid coefficient sets on the Fq value for [ ] is shown in Table 2-3. The initial line with a grid type of "None" provides the Fq values without a spacer grid model. [

]

Table 2-3

[ ] Fq Values for Various Inconel Grid Coefficient Sets

The impacts of the various Zircaloy spacer grid coefficient sets on the Fq value for [ ] are shown in Table 2-4 and Table 2-5, respectively. The initial line with a grid type of "None" provides the Fq values without a spacer grid model. [

]

Table 2-4

[ ] Fq Values for Various Zircaloy Grid Coefficient Sets

Table 2-5

[ ] Fq Values for Various Zircaloy Grid Coefficient Sets

Three of the results are discussed in further detail using Figure 2-1 through Figure 2-3. In each figure, the left axis indicates the power density while the right axis indicates the peaking change due to the spacer grids. [

]

Figure 2-1

Power Densities for [ ]

Figure 2-2

Power Densities for [ ]

Figure 2-3

Power Densities for [ ]

3.0 RAI 3

Question:

Section 3.2.2 of the TR discusses multi-group power form functions. However, the actual form of the functions is not presented. Power form functions are discussed in Section 3.7 of the original ARCADIA® TR ANP-10297P-A (Reference 3), specifically Equation 3-51, but these power functions are not multi-group. Confirm whether the power form functions presented in the original ARCADIA® TR are the same power form functions used in ARCADIA® Supplement 1 and, if applicable, indicate how they have been modified to accommodate a multi-group approach.

Response:

The power form functions presented in the ARCADIA® topical report (Reference 3) have been updated to be energy-group dependent values.

The intra-nodal (homogeneous) power is determined from the pin cell average fluxes and cross-sections for each energy group.

$$P_{n,g}^{hom} = \kappa \Sigma_{f,g,n} \phi_{g,n}$$

The local pin power for cell n is expressed as the product of the intra-nodal power distribution and single assembly multi-group power form functions. The power form functions are generated from APOLLO2-A calculations and stored in the cross-section library.

$$P_n = \sum_g P_{n,g}^{hom} f_{n,g}^{pow}$$

4.0 RAI 4

Question:

Section 3.6 of the TR discusses the incorporation of a control rod cusping model to overcome the "cusping" effect in axial flux distribution that results from performing volume-weighting of cross-sections in partially rodded nodes. The NRC staff understands the approach described in the TR and the equations presented, but there are no qualification results presented to justify the model's performance and correct implementation in the code. Provide before and after axial flux distribution plots and a brief description justifying the model's qualification.

Response:

The correctness of the control rod cusping model was verified using a representative test suite containing several test cases. Three test cases are presented here:

1. A 3D core with Cartesian node dimensions 20 x 20 x 20 cm, featuring a control rod bank that is gradually inserted fully from the top to the bottom of the core. This case has axial intra-nodal heterogeneities due to partial downward control rod penetrations in the nodal volumes.
2. This case is the same as the previous case but with a finer axial mesh (i.e., Cartesian node dimensions 20 x 20 x 10 cm).
3. This case is similar to the first case, except that the control rod consists of multiple axial material regions. This verification was pursued on whether the models smooths the reactivity curve according for a transition between two different control rod regions with varying boundaries between the two parts.

Case 1 was run with successive steady state calculations as the control rod is inserted into the core. Each steady state calculation used a critical boron search. The process was run with the control rod cusping model active and inactive. Figure 4-1 shows the critical boron concentration versus control rod insertion for an active rod cusping model (icrhet=1) and an inactive control rod cusping model (icrhet=0). Figure 4-2 shows the differential control rod worth using the same data. The control rod cusping model significantly improves (i.e., smooths) the differential control rod worth during the partial insertion within a nodal volume.

Case 2 was run in a similar manner as Case 1. Figure 4-3 and Figure 4-4 provide the critical boron concentration and the differential control rod worth versus insertion depth. Again, the control rod cusping model successfully smooths the differential worth of the control rod when it is partially inserted into a node.

Case 3 is used to verify the behavior when multiple control rod regions are used in the model. Figure 4-5 shows the critical boron concentration versus the boundary between the two axial regions of the control rod. When the boundary of the control rod aligns with the nodal boundary (40 and 60 cm in the figure), the results with the control rod active and inactive are equal. When the two regions are partially inserted in the node (between 40 and 60 cm), the active control rod cusping model provides a critical boron concentration without the cusping effect (has a more linear shape).

These test cases provide the verification that the control rod cusping model was correctly implemented for one or multiple regions and that it improved the differential rod worth for partial insertion in a node.

Figure 4-1
Critical Boron Concentration versus Control Rod Insertion, Case 1

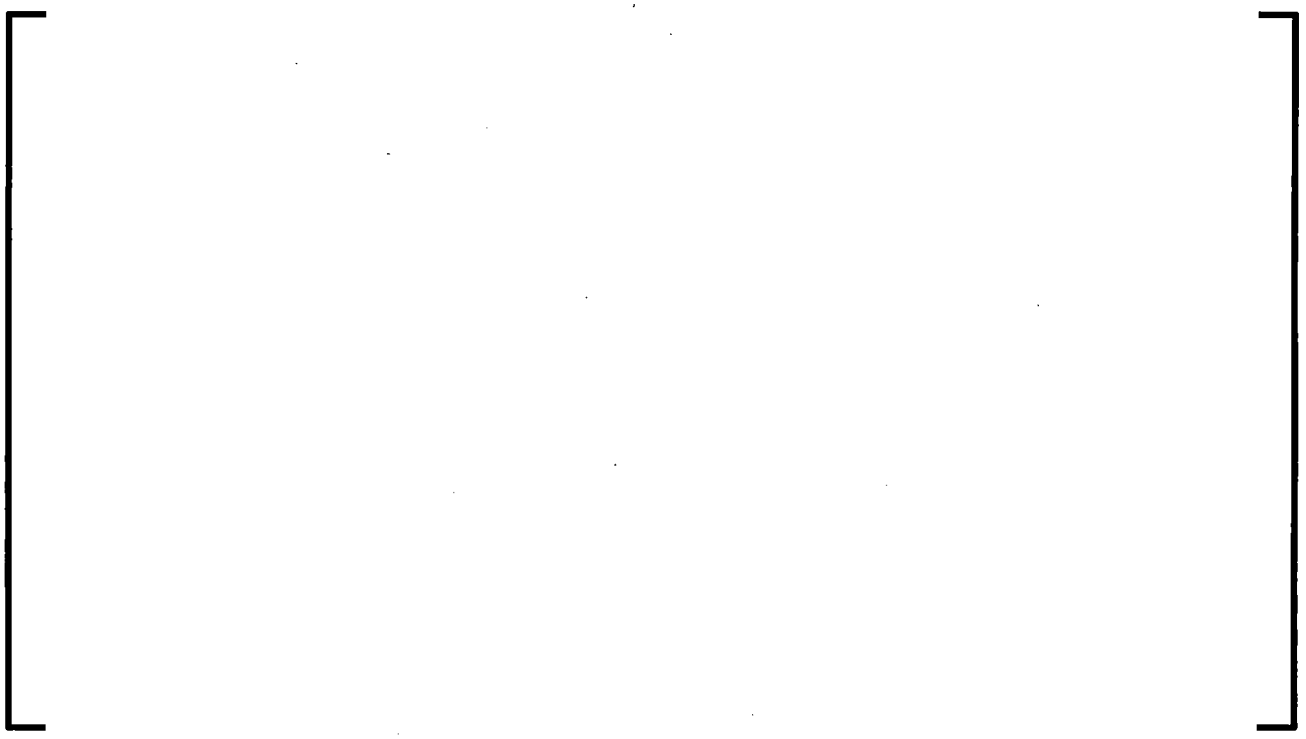

Figure 4-2
Differential Control Rod Worth versus Insertion, Case 1

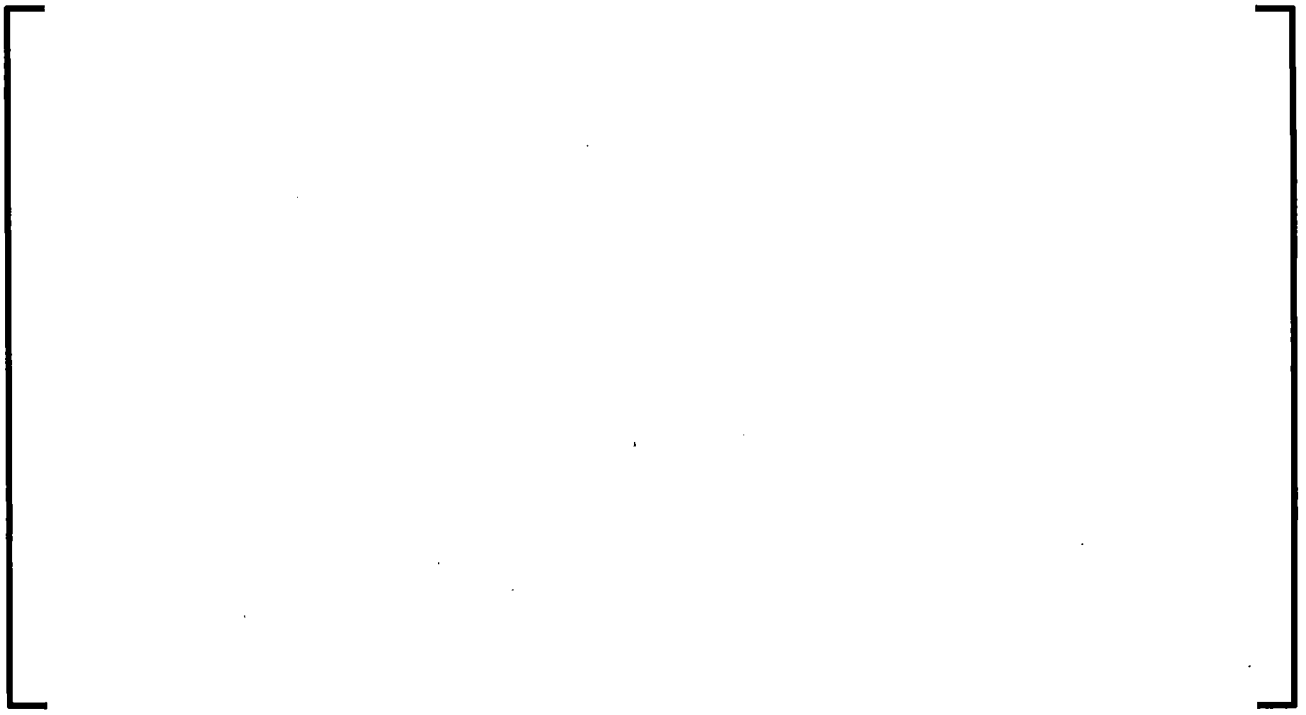

Figure 4-3
Critical Boron Concentration versus Control Rod Insertion, Case 2

Figure 4-4
Differential Control Rod Worth versus Insertion, Case 2

Figure 4-5
Critical Boron Concentration versus Multi-Region Control Rod Boundary Position, Case 3

[ ]

5.0 RAI 5

Question:

Section 3.9 of the TR describes how penalization of sensitive parameters is necessary for applying appropriate biasing, and how modifications were made to ARTEMIS™ to allow for adjustments of reactivity parameters and penalization of thermal-hydraulic and thermal-mechanical parameters. However, the modifications made to ARTEMIS™, the list of parameters that will be penalized, and how any penalization will be performed was not discussed. Before the NRC staff can assess the acceptability of these modifications with respect to ARCADIA®, this information must be supplied. Provide a discussion regarding how ARTEMIS™ was modified to allow adjustments of parameters, the parameters that will be adjusted and/or penalized, and the criteria guiding the penalization.

Response:

ARTEMIS™ was modified to allow penalization of the power distribution, neutronic response, thermal-hydraulic properties, and thermal-mechanical properties. The modifications consist of code options that may be activated to penalize the core behavior. These adjustments are used to account for uncertainties and to provide conservative allowances in an analysis. The parameters that may be adjusted and/or penalized are discussed below. The actual parameters that will be adjusted and/or penalized and the criteria for penalization will be addressed as part of the ARCADIA® methodology reports (e.g., ARITA). The intent of Section 3.9 was to inform the NRC that these options exist in the code and are intended to be used in upcoming methodology topical reports.

The power distribution may be penalized at various geometric levels that include the core, fuel assembly, fuel rod, and fuel pellet. These are typically implemented as direct multipliers to the power or the power distribution. The power distribution may be renormalized to preserve the total power. Alternatively, the modified power distribution may be kept such that the total power is increased. The axial power shape may be modified to provide a more penalizing initial condition for a transient. The code has options to search for a desired power offset condition by either modifying the xenon distribution or by adjusting the control rod insertion.

The general neutronic response may be penalized. This includes the moderator feedback, Doppler feedback, boron worth, control rod worth, delayed neutron fraction, inverse neutron velocity, and fraction of energy deposited directly in the coolant. ARTEMIS™ includes search options to determine cross section adjustments to obtain desired moderator, Doppler, and boron coefficients. The cross section adjustments are determined before a transient by running a series of calculations. The transient calculation then uses the cross section adjustments to implement the desired response for changes in the moderator, fuel, and boron state conditions. ARTEMIS™ provides a search option to determine a factor for the cross section change due to control rod insertion. This search determines the factor that will produce a desired k-effective and thus a desired control rod worth. The delayed neutron fraction, inverse neutron velocity, and the energy deposited in the coolant are penalized directly through the input for the calculation.

The main thermal-hydraulic conditions that may be penalized are the inlet flow, inlet temperatures, and system pressure. These penalties may be defined as a function of the time during a transient. The inlet flow and inlet temperature may depend on the radial location.

The fuel rod thermal conductivity and specific heat capacity may be penalized using a temperature-dependent function. Factors are applied over one or more temperature ranges. A transition interval is defined between each range to maintain a smooth behavior of the thermal conductivity and specific heat capacity versus temperature. The radial power distribution with the fuel pellet may be penalized. A coefficient is applied to standard radial power distribution that either increases the rings with relatively high power or flattens the radial power distribution. The effect of oxidation on the fuel rod behavior may be treated either with a direct penalty on the fuel rod property (such as thermal conductivity). Alternatively, the code allows the definition of an oxide thickness versus the fuel pellet burnup. This thickness is then used to modify the fuel thermal properties. The gap conductance between the fuel pellet and the cladding may be penalized directly through modification of the gap conductance tables. Alternatively, the penalization may be defined as a function of the fuel pellet burnup for each fuel pellet type.

6.0 RAI 6

Question:

Section 3.10 of the TR describes incorporation of time-step control during transient calculations via use [

] The NRC staff is familiar with a similarly-described time-step control method from AREVA's AURORA-B methodology (Reference 4), but without confirmation of any ARCADIA®-specific differences between the implementations, the NRC staff cannot independently rule-out time-step related code convergence issues. Confirm whether the time-step control approach used in ARCADIA® is different from that of AURORA-B and, if so, provide a description of how time steps are chosen for the [

] In either case, what are the ranges of time-steps allowed?

Response:

The time step control for the nodal core simulator MB2-K of AURORA-B uses a predictor-corrector method to evaluate the rate of change of the core average fission power. The new time step is determined as a fraction of the previous time step when the "corrector" core average fission power is significantly different from the "predictor" core average fission power.

The ARTEMIS™ time step control method is based on [

]

[
]

[
]

7.0 RAI 7

Question:

Section 3.13 of the TR describes the incorporation into ARTEMIS™ of an excore detector model that makes use of a set of weighting factors to calculate the excore detector response. The model also makes use of a temperature decalibration model. However, the formulation of the weighting factors and the temperature decalibration model are not provided. Without this information, the NRC staff cannot assess the adequacy of the excore detector model. Provide a mathematical description and a discussion of how the weighting factors are determined and how the temperature decalibration model functions.

Response:

Excore Weighting Factors

Two-dimensional excore weighting factors are generated outside of ARCADIA® using a discrete ordinates code (i.e., DORT). DORT solves the Boltzmann transport equation with the adjoint flux in cylindrical geometry. The adjoint solution to the excore detector model is performed with a unit flux incident upon the detector. P_3 cross section expansion and S_8 quadrature approximation are employed.

The method to perform the calculation with DORT is similar to that provided in Reference 6. The assembly specific weighting factors are:

$$W_j = \int_{\Delta V_j} W(r)dr$$

where

W(r) is the weighting factor for the detector response at position r

ΔV_j is the volume of assembly j

The calculated W_j values are then normalized such that $\Sigma W_j = 1.0$.

An example of the geometry used in the DORT calculation is provided in Figure 7-1.

Activity values are extracted from the DORT calculations and adjusted by the ratio of assembly cross-section area meant to be modeled to the assembly area actually modeled:

$$A_{adj}=A_{DORT} \times \frac{V_{act}}{V_{DORT}}$$

where

A_{DORT} is the activity extracted from the DORT output

V_{act} is the actual assembly volume

V_{DORT} is the volume used in DORT and extracted from output

Normalized weighting factors for each assembly location are calculated by dividing the volume adjusted activity for each assembly by the total volume adjusted activity of all assemblies.

Interior locations have a small contribution to the excore detector response. Therefore, final normalized weighting factors are calculated using only the assemblies with higher normalized weighting factors. This is accomplished by renormalizing the weighting factors for the assembly locations that had higher normalized weighting factors (typically ≥0.01).

A similar process may be used to determine axial excore detector response values.

Excore Model

The ARTEMIS™ excore detector model predicts the axial flux difference (AFD) that is seen by the excore detectors. The following response equation is used. This model supports a top and bottom detector at four radial locations.

[

]

where

[

]

The calibration factor is either input or calculated by ARTEMIS™, if requested. ARTEMIS™ determines the calibration factor that either (a) matches the core power, or (b) matches the core average AFD based on the core power distribution. The radial and the axial weighting factors are input items. The coolant temperature correction function is defined by the following equation.

[

]

where

[ ]

The top and bottom detector temperatures are calculated from the following equations.

[ ]

where

[ ]

The power fraction in each detector is calculated using the following equation, where N_{det} is the number of excore detectors (typically 4).

[ ]

The simulated excore AFD for each detector is then simply defined by the following equation:

[ ]

The total excore AFD is defined as the numerical average of the AFD values from the 4 excore detectors:

$$AFD_{ex}^{tot} = \frac{\sum AFD_{ex}}{4}$$

Temperature Decalibration Model

The temperature decalibration model is an optional feature of the excore model that was not used in the calculations in Reference 1. It is intended for use with online core monitoring applications. Therefore, the temperature decalibration model option is not being requested for review and approval.

Figure 7-1
Example of DORT Geometry

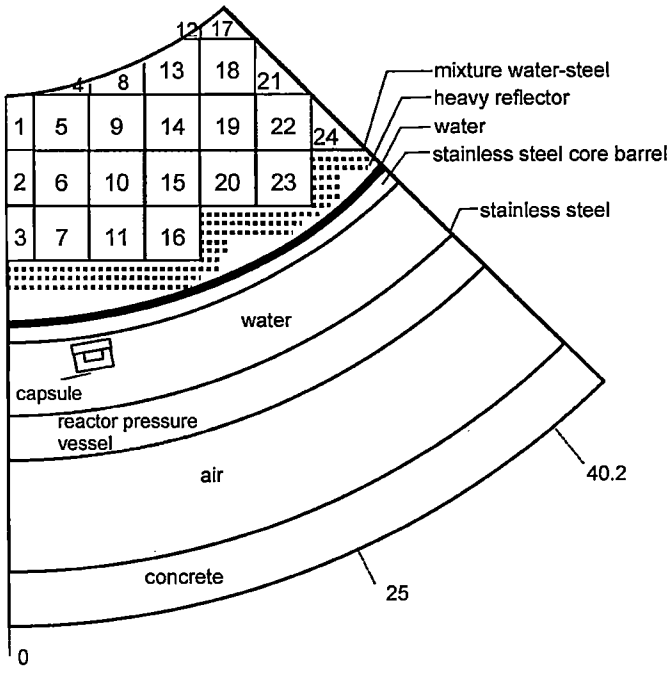

8.0 RAI 8

Question:

Table 8-1 in Section 8.2.1 of the TR lists the "Observed" and "Measured" deviations for a number of Babcock and Wilcox Company (B&W) 1980's critical core configurations, both of which are used to determine the uncertainty due to calculations alone. The Observed Deviations are actually generated from ARCADIA®-predicted results that are presented in Figures 4-5 through 4-10 of the TR. These figures also include the B&W experimental data from which, presumably, the Measured Deviations are generated. However, when utilizing the experimental data presented in the figures, the NRC staff was unable to reproduce the Measured Deviations presented in the table. One possible explanation is that a lower-sided 95 percent tolerance limit on the standard deviation of the experimental data may have been used when producing the Measured Deviations in the table. This would result in a maximized calculation uncertainty. However, when determining the confidence interval that covers 99 percent of the data with a 95 percent confidence, the NRC staff found the values presented in Table 8-1 appear to be off by a factor of 10. Given this discrepancy, the NRC staff cannot confirm the accuracy of the supplied data and therefore cannot confirm the magnitude of the uncertainty due to ARCADIA®'s calculations. Provide a description of how the Measured Deviations in Table 8-1 were generated. Include in the description whether a tolerance interval was used, what percentage of the data the interval covers, and the confidence level used when performing the calculation. Additionally, confirm whether or not the experimental B&W 1980's Critical Core data provided in Figure 4-5 through 4-10 are the same data used to generate the Measured Deviations in Table 8-1. If these data were not used in the generation of the Measured Deviations, provide a copy or a reference to the actual data used.

Response:

The experimental B&W 1980's Critical Core data provided in Figure 4-5 through 4-10 are the same data used to generate the Observed Deviations in Table 8-1. There is not sufficient information in the data from Figures 4-5 through 4-10 to estimate the measured deviations. The measurement uncertainty is estimated using the measurements for the B&W 1980's Critical Core Benchmarks in Reference 7. Three tests for each core configuration were performed. The reported pins were measured for each test that yielded three measurements for each pin. The average of the three tests is the reported values for the measurements. The variation of the three measurements is used to estimate the measurement error. The data for these measurements can be found in Table 4-6, Table 4-7, Table 4-8, Table 4-9, Table 4-10, and Table 4-11 in Reference 7 for cores 1, 5, 12, 14, 18, and 20, respectively. The power of the Gad pins is very low, is not limiting, and is not included in the statistics.

The statistical evaluation of these results is described:

A W-test (Page 76 in Reference 8) is performed on each of the three measurements and the hypothesis that the error distribution is normal is not rejected. Hence, the underlying distribution can be assumed as normal.

For a given core, the three measurements of each pin ($m_{i,l}$) are processed via the following equations to calculate the measurement standard deviation.

Definitions and equations:

$$m_{i,l} = measurement\ of\ each\ pin\ i\ for\ test\ run\ l$$

$$\overline{X_i} = Average\ of\ 3\ measurements\ for\ pin\ i$$

$$n = number\ of\ pin\ powers\ measured$$

$$average\ relative\ variance\ of\ the\ 3\ test\ runs\ for\ pin\ i\ = S_i^2$$

$$= \frac{1}{2} \times \sum_{l=1}^{3} [\left(\frac{m_{i,l} - \overline{X_i}}{\overline{X_i}}\right) \times 100]^2 / 3$$

$$pooled\ variance\ for\ the\ core = S^2 = \frac{\sum_{i=1}^{n} S_i^2}{n}$$

$$degrees\ of\ freedom = \ v = (3-1) * n$$

$$S = Estimated\ measurement\ uncertainty$$

Since a conservatively high calculational uncertainty is desired and the measurement uncertainty is removed from the observed uncertainty to get the calculational uncertainty, a conservatively low measurement uncertainty is obtained.

Based on Table A-21 and Section 2-2.3.2 of Reference 9, the low estimate of the measurement uncertainty for each core can be obtained by:

$$Measurement\ Error\ Reported\ in\ Table\ 8-1 = S_L = \ A_p * S$$

$$A_p = \ \sqrt{2v}/(z_p + \sqrt{2v-1}) \text{ for large degrees of freedom}$$

where

v is the degrees of freedom

z_p is defined in Table A-2 of Reference 9. It is equal to 1.645 for a 95% confidence that the true error σ is larger than the one sided lower confidence limit

Thus, it can be asserted that there is a 95% confidence that the real measurement uncertainty is greater than the reported measurement uncertainty.

Example:

The lower confidence limit is calculated for the following ten pins with three independent measurement runs:

Measurement (i)	Run 1 ($m_{i,1}$)	Run 2 ($m_{i,2}$)	Run 3 ($m_{i,3}$)	Average ($\overline{X_i}$)	$S_i^2 = \frac{1}{2} \times \sum_{l=1}^{3} [\left(\frac{m_{i,l} - \overline{X_i}}{\overline{X_i}}\right) \times 100]^2 / 3$
1					
2					
3					
4					
5					
6					
7					
8					
9					
10					

Number of measurements = n

Pooled variance = $S^2 = \frac{\sum_{i=1}^{n} S_i^2}{n}$

Estimated measurement uncertainty = $\sqrt{S^2}$

Since v = 2*n = [ ] degrees of freedom the lower confidence limit is:

$$S_L = A_p * S$$

$$A_p = \frac{\sqrt{2v}}{z_p + \sqrt{2v - 1}}$$

[ ]

For this example, the exact value of $A_{0.05}$ can be obtained by looking up the value for v = [ ] degrees of freedom in Table A-21 of Reference 9.

From the Table: $A_{0.05}$ = [ ] and S_L = [ ] The closeness of the estimated $A_{0.05}$ value from using the A_p formula given above at v = [ ] to the tabulated exact $A_{0.05}$ value justified the degrees of freedom (shown below) for the B&W 1980's Critical Core data are large enough to use the above A_p formula.

Experiment	Degrees of Freedom
Core 1	[ ]
Core 5	
Core 12	
Core 14	
Core 18	
Core 20	

9.0 RAI 9

Question:

Sections 8.3.1 and 8.3.3 of the TR state that global and local uncertainty components associated with the MEDIAN reconstruction methodology are combined to estimate "the Normal Uncertainty and Non-Parametric Uncertainty." However, the exact approach used to combine the uncertainty components and estimate the Normal and Non-Parametric uncertainties is not explicitly stated. Provide a discussion of, or a reference to, the technique used to combine the uncertainty components.

Response:

The technique used is the same as described in the response to RAI 47 in ANP-10297P-A (Reference 3).

10.0 RAI 10

Question:

Section 8.1 of the TR states that when determining 95/95 (95 percent confidence for 95 percent of the data) tolerance limits "Monte Carlo simulations are performed on the actual distributions to obtain a 95/95 tolerance limit which does not require the data to be normally distributed." This is also known as a Non-Parametric Uncertainty analysis. The NRC staff has investigated this technique and found that the results of this process are sensitive to the manner in which the input distributions are sampled. Specifically, sampling from a reduced range of the input distributions, such as within plus or minus 2 sigma (±2σ), does not reasonably predict the 95/95 tolerance limit that is produced when sampling from the full range of the input distributions. When performing the Non-Parametric Uncertainty analysis for production cases, what is the range AREVA will use when sampling the input distributions?

Response:

[

]

11.0 REFERENCES

1. ANP-10297P(A), Revision 0, Supplement 1, The ARCADIA® Reactor Analysis System for PWRs Methodology Description and Benchmarking Results, June 2015.
2. Letter from J. Rowley (NRC) to G. Peters (AREVA), "Request for Additional Information Re: AREVA Inc. Topical Report ANP-10297P(A), Revision 0, Supplement 1, 'The ARCADIA® Reactor Analysis System for PWRs Methodology Description and Benchmarking Results' (CAC No. MF6469)," April 18, 2017.
3. ANP-10297P-A, Revision 0, The ARCADIA® Reactor Analysis System for PWRs Methodology Description and Benchmarking Results, February 2013.
4. ANP-10300P, Revision 0, "AURORA-B: An Evaluation Model for Boiling Water Reactors; Application to Transient and Accident Scenarios," December 2009.
5. N. Crouzet and P. Turinsky, "A Second-Derivative-Based Adaptive Time-Step Method for Spatial Kinetics Calculations," Nuclear Science and Engineering, Vol. 123, June 1996.
6. H. Tochihara, E. Ochiai, and T. Hasegawa, "Reevaluation of Spatial Weighting Factors for Ex-Core Neutron Detectors", Nuclear Technology Vol. 58, August 1982, American Nuclear Society.
7. L.W. Newman et al., "Urania Gadolinia: Nuclear Model Development and Critical Experiment Benchmark", DOE/ET/34212-41, BAW-1810, April 1984.
8. John L. Jaech Statistical Methods in Nuclear Material Control, United States Atomic Energy Commission, 1973.
9. Mary G. Natrella, Experimental Statistics, NBS Handbook 91, National Bureau of Standards, 1963.